'Green barriers' for air pollutant capture: leaf micromorphology as a mechanism to explain plants' capacity to capture particulate matter

María del Carmen Redondo-Bermúdez[a]*, Idris Tugrul Gulenc[b], Ross W. Cameron[a], Beverley J. Inkson[b]

a. Department of Landscape Architecture, The University of Sheffield, The Arts Tower, S10 2TN Sheffield, UK
b. Department of Materials Science and Engineering, The University of Sheffield, Mappin Street, S1 3JD, Sheffield, UK

*Corresponding author
E-mail address: maria.redondo@sheffield.ac.uk

1 Abstract

Finding ways to mitigate atmospheric particulate matter (PM) is one of the key steps towards fighting air pollution and protecting people's health. The use of green infrastructure could help to improve urban air quality and to promote more sustainable cities. Detailed knowledge of how plants capture particulate matter can support plant selection for this purpose. Previous studies have primarily focused on 2D techniques to assess the micromorphology of plant leaves. Here, 3D optical profilometry and SEM imaging (2D) are used to quantify leaf roughness and other micromorphological leaf traits of three contrasting plant species (*Hedera helix* 'Woerner', *Thuja occidentalis* 'Smaragd', and *Phyllostachys nigra*) located within a mixed green barrier. These techniques have allowed us to identify the relative distribution of adhered atmospheric PM with respect to the surface topography of leaves, with high spatial resolution. Leaf surface roughness did not show a direct relationship with PM deposition; however, the descriptors width, depth and frequency of the grooves are important to explain PM capture by the leaves. Additionally, the presence of wax on leaves was relevant for PM adherence. All species captured PM, with their overall PM capture efficiency ranked from highest to lowest as follows: *Thuja occidentalis* > *Hedera helix* > *Phyllostachys nigra*. All green barrier species contributed to air quality improvement, through PM capture, regardless of their location within the barrier. Having multiple species in a green barrier is beneficial due to the diverse range of leaf micromorphologies present, thus offering different mechanisms for particulate matter capture.

Key words: air pollution, ecosystem service, leaf roughness, $PM_{2.5}$, urban plants.

2 Introduction

Particulate matter (PM) is considered one of the most harmful air pollutants to human health. In the urban environment, the sources of outdoor particulate matter are primarily related to combustion, for instance, from landfill waste incineration, domestic wood burning, industrial activities or petro-chemicals from motorised vehicle traffic (WHO, 2019). The use of vegetation to help mitigate urban air pollution has been explored and applied in recent years as part of the 'nature-based solutions' agenda (European Commission, 2015, McDonald et al., 2016). The growing evidence of plants (green infrastructure) to improve air quality has led to the research of more plant species and combinations to be used in the outdoors urban environment.

It is known that trees and hedges can block and divert airflow containing air pollutants (Hewitt et al., 2019), inhibiting them from accumulating and reaching harmful PM levels. Additionally, PM can be captured by the large surface area of foliage (McDonald et al., 2007), acting as a filter to clean desired areas. The variation in foliage type between species can foster or hinder particle deposition; specifically, the micromorphology of the leaves' surface can impact their ability to capture PM (Zhang et al., 2018). Therefore, it is important to consider leaf micromorphology for the selection of plants for air quality improvement.

The micromorphological traits of plants as a taxonomic function have been extensively studied using Scanning Electron Microscopy (SEM) due to its high-magnification imaging (Yigit, 2017). Ottelé et al. (2010) were pioneers in the development of a methodology for the use of SEM to quantify PM pollution on leaf surfaces. This technique has been used to investigate which are the most conducive micromorphological leaf traits for PM capture in a limited number of plant species (Chen et al., 2017; Weerakkody et al., 2018a; Wang et al., 2019; Zhang et al., 2019; He et al., 2020). Some studies suggest that the most influential micromorphological features for PM retention are leaf surface roughness, presence of trichomes/hairs, cuticular wax, and stomatal density (Weerakkody et al., 2017; Zhang et al., 2018). However, the details and descriptors of leaf roughness for PM capture are still unclear, especially because the topography of leaves is complex in three dimensions (x, y, z).

SEM imaging provides very valuable information on leaf micromorphology and PM location. It is limited to two dimensions, however, causing depth and height of grooves not to be taken into consideration when attempting to identify the locations where particles get deposited. Here, to deepen the understanding of foliar micromorphology, SEM imaging (2D) is combined with 3D surface profiling, which can help to analyse if leaf surface roughness is a factor that influences PM capture, distribution, and retention. Specifically, 3D optical profilometry is used to quantify local leaf roughness across adaxial and abaxial leaf surfaces for different species and evaluate if surface roughness is a key factor in PM capture.

In this study, we aim to identify the variation in air pollution-filtering mechanisms of three plants (*Hedera helix* 'Woerner', *Thuja occidentalis* 'Smaragd', and *Phyllostachys nigra*) that are part of a mixed green barrier in a school playground. SEM and 3D optical profilometry enable determination of the micromorphological traits of each plant species, especially the details of local leaf surface roughness, and PM capture capacity. Specifically, the combined techniques allow us to answer the following research questions: 1) Does leaf surface roughness correspond to higher particle capture? 2) Do the micromorphological mechanisms of PM capture differ within the green barrier plants? 3) Under similar exposure conditions, does PM density differ within the green barrier plants?

3 Materials and Methods

3.1 Study site and sampling

The plant species under study are part of a green barrier installed during late October 2019 around a school playground in south west Sheffield, UK. The 60 m green barrier was constructed using different plant taxa and arranged in two layers to serve as a physical barrier to divert pollutants in the local airflows. We selected a green barrier section that comprises three key taxa with different leaf morphologies: *Hedera helix* 'Woerner', *Thuja occidentalis* 'Smaragd' and *Phyllostachys nigra* (see Table 1 in supplementary information). The former two plants are specific cultivars of ivy and white cedar, correspondingly, and the latter is a particular species of bamboo. Here, they will all be referred to as species.

The selected green barrier section is located within 2.5 m of a street with vehicle traffic. The plant species are arranged in the space as a *Hedera helix* climber fence facing the street, immediately followed behind by five specimens of *Thuja occidentalis* and four of *Phyllostachys nigra* that are situated less than 10 cm apart from the climber. The *H. helix* plants climb up a metal grid up to 2.20 m height, whilst the *T. occidentalis* and *P. nigra* are semi-mature specimens of around 2.40 m in height (Fig. 1). Gaps within the *Hedera* (Fig 1c), also result in some of the lower leaves of *Thuja* and *Phyllostachys* being directly exposed to the roadside conditions. On the 24th of February 2020, eight leaf samples oriented towards the street were manually collected from each species for SEM analysis; and on the 12th of August 2020, a second sampling event of two leaves per species took place to complement the 3D optical profilometry observations. Mature and healthy leaves sampled at 1.25 m from the ground were stored in plastic containers, attaching the stem to the bottom of the container to prevent movement during their transportation to the laboratory. Samples were stored until lab analysis within two days.

For the inner-city school, potential local sources of particulate matter pollution are motorised vehicle traffic and woodstove burners from residences and businesses close to the school. Based on the flow of vehicles passing through a traffic sensor, approximately 5,200 cars/day circulated on the street adjacent to the green barrier during February 2020 [dataset] (Urban Flows Observatory at The University of Sheffield, 2020). PM pollution at the study site was assessed using an air quality monitor (AQMesh MK3, Environmental Instruments Ltd, UK), which is fixed inside the playground to give continuous measurements, every 15 min. The air quality monitor uses an optical particle counter to calculate PM mass-based fractions. During the two weeks prior to leaf sampling in February, the study site's particulate matter pollution averaged (± SE) 0.49 ± 0.02 $\mu g\ m^{-3}$ for PM_1, 2.01 ± 0.08 $\mu g\ m^{-3}$ for $PM_{2.5}$, and 7.95 ± 0.26 for $\mu g\ m^{-3}$ PM_{10}. The weather conditions during those two weeks were standard for the winter season in Sheffield: light but constant rain and temperatures below 10 ^oC. The weather station on site (WS700-UMB, Lufft, Germany) recorded rain 24% of the time with an average intensity of 0.38 (± 1.05) mm h^{-1}, and the temperature averaged 6.13 (± 2.50) ^oC.

3.2 Leaf micromorphology analysis

The collected green barrier leaf samples were examined by Scanning Electron Microscopy (Hitachi TM3030Plus SEM, Japan). Three leaves per species were used to image the adaxial side and three different leaves to image the abaxial side. Sections of 5.0 x 5.0 mm for broadleaves (*H. helix* and *P. nigra*) and 5.0 mm long for the conifer (*T. occidentalis*) were cut from each chosen leaf and observed by SEM using back scattered electron (BSE) imaging in low vacuum mode (15 kV). No conductive coating was applied to the leaves. Micrographs of three randomly chosen spots per leaf section were taken at two magnifications, 600x and 1,200x, accounting for108 micrographs in total.

Leaf samples imaged at 600x and 1,200x were examined for their micromorphological traits. The primary descriptors included surface structures, trichome and hair presence, wax presence, leaf roughness and stomatal density (stomata mm^{-2}). The latter was quantified by counting the number of stoma per unit leaf area of the SEM images, as in Sgrigna et al. (2020):

$$Stomatal\ density = \frac{Stomata\ count}{SEM\ micrograph\ area} \qquad (1)$$

Leaf topography was examined in 3D using optical profilometry (ContourGT, Bruker, USA). Quantitative 3D surface profiling of the examined leaves allows determination of leaf roughness values in chosen locations, and assessment of local topographic features, including the 3D shapes, sizes and repetition distances of grooves, creases, stomata and hairs on the leaf surfaces. Areal average roughness (S_a), a standard roughness parameter for manufacturing, was used to quantify roughness of leaves. The higher the S_a value, the higher the roughness. The areal average roughness (µm) is defined as below (Hutchings and Shipway, 2017), where Z_i denotes height of each point, and N denotes number of measured points:

$$S_a \cong \frac{1}{N}\sum_{i=1}^{N}|Z_i| \qquad (2)$$

For a given leaf surface profile, the maximum peak height (S_p) and maximum valley depth (S_v) were used to determine the maximum and minimum points within the data, and to assess macroscopic curvature of the examined leaf samples. Here, masked leaf regions of 250x250 µm area were used for S_a, S_v and S_p calculation, in order to remove no-signal points around the edges of measurement frames. A Gaussian regression filter was used to remove leaf curvature (low frequency modulation), and roughness values are presented with and without this filter. The application of the Gaussian filter enabled the assessment of the contributions to the leaf roughness from both the broad underlying curvature of the leaf and its localised grooves and ridges.

3.3 Foliar particulate matter density and distribution analysis

The lower magnification 600x SEM leaf images were selected for quantitative analysis of PM count, size and location. In the SEM images, particulate matter could be identified due to higher BSE emission (bright spots) compared to the underlying leaf (darker background) (see Fig. 1 of Supplementary Information). The higher local BSE emission originates from a local chemical composition with higher average atomic-number (Z) compared to surrounding material, or from topographic contrast due to surface edges/regions inclined to the incident e-beam. In this case, the BSE contrast of PM arises primarily from chemical Z-contrast compared to the leaf, which might include combustion products containing metal constituents. For the analysis conditions used, namely BSE imaging and 600x magnification for large area statistical PM analysis, particles <0.2 µm in diameter cannot be identified. These might entail some semi-volatile organic compounds, some sulfuric acid derived compounds, and some organic/carbon PM with chemistry close to the leaf (Harrison, 2020).

The SEM micrographs were processed with ImageJ software - FIJI project (Schindelin et al., 2012), to count the number of particles on each leaf section. Each micrograph was subjected to the unsharp mask, thresholded with the auto threshold tool to minimise researchers' bias, and then processed with the fill and watershed tools before particle analysis. For each quantified particle, the diameter was computed directly from SEM particle image analysis following the same assumptions as in Ottelé, Bohemen and Fraaij (2010), who did not allocate a limit to the circularity value in order to include all various particle shapes.

Taking into account the spatial resolution limit of the micrographs (0.2 µm for 600x and 0.1 µm for 1200x), the particles were then assigned into one of the following categories: PM_1 (from 0.2 to 1 µm), $PM_{2.5}$ (>1 to 2.5 µm) and PM_{10} (>2.5 to 10 µm). The Total Adhered Particles (TAP) is the total sum of the PM categories. The particulate matter investigated here is of size dimensions that can be affected by leaf roughness.

Particulate matter areal number density (PM mm^{-2}), referred to here as PM density, was calculated for each species and each leaf side as follows:

$$PM\ density = \frac{PM\ count}{SEM\ micrograph\ area} \qquad (3)$$

The imaging and PM density analysis followed was systematically the same for all leaf-types to determine trends between the different plant species. The results derived from these represent PM deposited on the leaves and are not equal to atmospheric PM concentrations.

3.4 Statistical analysis

Statistically significant differences between PM density by species and leaf side were analysed using the R statistical software version 3.6.3 (R Core Team, 2020). The PM density data presented a Gaussian curve behaviour skewed to the right; therefore, non-parametric tests were used to assess statistically significant differences. The Kruskal-Wallis ranks sum test was used to assess the variation in PM density among different plant species, proceeded by post hoc Dunn's test, using the Bonferroni correction. The Wilcoxon rank sum test was used to identify PM density variation between the adaxial and abaxial side of the leaves. Statistical difference was considered at $p < 0.05$ value.

4 Results

4.1 Leaf micromorphology

4.1.1 Leaf surface

Optical and SEM imaging of the green barrier plants revealed markedly diverse structures on the leaves of the different species. *Hedera helix* showed abundant tubular grooves on the adaxial and abaxial sides of the leaves (Figs. 2a,b), and a network of fibres on both sides which was more prominent on the abaxial surface (Fig. 2d). Muhammad et al. (2020) reported that *H. helix* is covered in epicuticular wax of platelet shape, which was not clearly defined in our uncoated samples. The stomata were ~12 μm long, and the guard cells surrounding them formed an oval of ~30 μm in diameter with a deep edge.

Thuja occidentalis exhibited rectangular-shaped aligned ridges of irregular sizes, from 5-50 μm long (Fig. 2e). The surface also had a network of fibres like on *H. helix*, but the fibres were less frequent (Fig. 2f). Both leaf sides were covered in a dense wax layer, which was difficult to observe in detail as it tended to melt under the intensity of the SEM beam at high magnification (Fig. 2g). According to Muhammad et al. (2020), the epicuticular wax of most conifers is tubular in structure. The stomata were ~10 μm long and were surrounded by a raised ring of guard cells of ~20-40 μm in diameter.

Phyllostachys nigra had the most notable variation between the adaxial and abaxial sides. The adaxial surface comprised 50-80 μm long, well-regimented aligned cells with undulate margins that interlock neatly with each other. The interlocking cells were located between, and aligned with, the ribs (Fig. 2i) and sometimes interspersed with potential silica bodies (Figs. 2i,k), typical of the Poaceae family (Vieira et al., 2002). The abaxial side also had a distinctly aligned structure, but with a visually more complex surface with protuberances and occasional microhairs (Figs. 2j,l). Both leaf sides displayed a sparse fibres network on their surface. The stomata were ~10 μm long, with the surrounding oval guard cells appearing slightly recessed with respect to nearby cells (Fig. 2l).

4.1.2 Stomatal density

Stomatal density varied considerably among the three species. Stomata were found only in the abaxial side of *H. helix* and *P. nigra* leaves, as they are part of the so called hypostomatous leaves (Xiong and Flexas, 2020). *H. helix* exhibited a well dispersed distribution of stomata, which were ~20-80 μm apart in the studied samples, with random aperture orientation but radial to a central principal stoma. Stomata in *P. nigra* occurred in aligned lines with a zig-zag pattern (Figs. 2j,k) having ~15-30 μm between each stoma, and ~60-80 μm between lines. On the contrary, both leaf sides of *T. occidentalis* had stomata, with uneven separation among them and located close to the intersection between the scales that form the leaf (Figs. 2e,h). It is known that slow-growing species like gymnosperms are part of the amphistomatous leaf group (stomata in both sides of the leaves) (Drake et al., 2019), and our studied conifer falls in this category. Despite having stomata in both surfaces, *T. occidentalis* showed the lowest mean stomatal density of 36.82 ± 12.43 stoma mm^{-2}, being eleven times less than *P. nigra* 413.49 ± 21.19 stoma mm^{-2}, which had the highest density. *Hedera helix* had stomatal density values of 207.69 ± 9.30 stoma mm^{-2}, approximately half of *P. nigra* (Table 1).

4.1.3 Leaf roughness

4.1.3.1 Leaf curvature

Leaf shape and local roughness was measured for the three species using 3D optical profilometry. Due to gentle macroscopic leaf curvature, it was evident that *T. occidentalis* (adaxial side) had the greatest variation in leaf surface height (Fig. 3e). *Hedera helix* (Fig. 3a) was intermediate in this effect, with *P. nigra* (Fig. 3.i) having the least macroscopic leaf curvature and surface height variation.

4.1.3.2 Micromorphological level

A Gaussian filter was used to remove the broad leaf curvature in order to better analyse the variations in local leaf roughness (Figs. 3,4). Leaf roughness at the micromorphological level (S_a) was greatest for abaxial *P. nigra* from all samples. Roughness for both adaxial and abaxial surfaces were in the order: *P. nigra* > *H. helix* > *T. occidentalis* (Table 1). Despite showing the same order, the magnitude of S_a varies considerably based on leaf side. On the adaxial surface, *P. nigra* ($S_a = 0.83$ μm) is slightly rougher than the other two species; whereas on the abaxial side, its roughness ($S_a = 2.57$ μm) doubles that of *H. helix* and is four times greater than *T. occidentalis*.

The abaxial surface of *P. nigra* had the largest distance between maximum peak height (S_p) and valley depth (S_v), of 28.89 μm. The leaf structure comprises a complex pattern of aligned papillae, stomata and grooves (Fig. 3l) that creates a large deviation from the mean line, leading to the highest S_a. The second highest roughness was found for the abaxial side of *H. helix*. Here, the presence of raised stomata and guard cells (Fig. 3d) and the size of the deepest groove ($S_v = -20.53$ μm) increase the deviation from the mean line. For both, *P. nigra* and *H. helix*, leaf surface roughness was greater on the abaxial side than on the adaxial side. In comparison, *T. occidentalis* had the lowest roughness at the micromorphological level from all species. Its grooves and ridges are less pronounced, ranging from 4 to -2.5 μm depth, and it has no evident deep structures except for stomata (Fig. 3g); which led to a high S_v on its adaxial side (Table 1).

The 3D optical profilometry height maps enable surface height line profiles to be extracted across surface features (Fig. 4). The surface height line profiles reveal notable differences in the size and shape of the micromorphological traits, among species. *H. helix* showed deep grooves of approximately ≤5 to 10 μm width and -2 to -18 μm depth (Fig. 4a), and its stomata are deep, reaching -20 μm depth (Fig. 4b). Similarly, *T. occidentalis*, had grooves of mostly ≤5 to 10 μm width (Fig. 4d); however, they were shallow (-1 to -2.5 μm depth); except for stomata which were deeper and wider (~-11 μm depth and ~10 μm width) (Fig. 4c). For *P. nigra,* besides the large surface height difference among its structures, the profiles showed wider grooves ranging from ≤5 to 18 μm width, and these were predominantly above the mean height line because they are created by the raised nearby structures (Figs. 4e,f).

4.2 Foliar particulate matter density and distribution

Particulate matter deposited on the leaves showed a broadly homogeneous distribution of the different fractions for all species (Fig. 5). Regardless of the leaf side, the surfaces were highly dominated by PM_1, with a proportion of particles identified ranging from 78.76% to 80.26% among species. In comparison, $PM_{2.5}$ and PM_{10} had a much lower number ratio; with $PM_{2.5}$ ranging from 11.6% to 17.63%, and PM_{10} ranging from 2.21% to 4.60% of particles (Table 2). Here the spatial resolution limit of the identified particles/particle clusters in the PM_1 category is 0.2 μm (micrographs at 600x magnification). The particles smaller than 0.2 μm which are not detected would further increase the PM_1 proportion, further emphasizing the identified trend of PM_1 > $PM_{2.5}$ > PM_{10} number ratio of captured particles.

SEM imaging revealed that the primary location of adhered PM was in recessed troughs, grooves and edge features (e.g. Fig. 2c), with particularly striking PM capture by the groove around stomata in *H. helix* (e.g. Fig. 2b). Particles were also found at the network of fibres that all species had on their leaf surface (e.g. Figs. 2d,f), and occasionally on protuberances in *T. occidentalis* and *P. nigra* (e.g. Fig. 2j).

Thuja occidentalis had the greatest PM density, when data is combined for both adaxial and abaxial surfaces (Table 3). This was the case for all size fractions. PM density was significantly greater for PM_1 and TAP compared to the two other species. Nevertheless, PM density of $PM_{2.5}$ and PM_{10} fractions were significantly greater for *T. occidentalis* only when compared to *P. nigra*, but not *H. helix*. This fact seems to indicate that both *H. helix* and *T. occidentalis* perform adequately at capturing small PM, but that additional mechanisms promote higher PM capture of the larger fractions for *T. occidentalis*.

Except for PM_1 on *H. helix,* the adaxial side of leaves appeared more effective at capturing PM than the abaxial side (Table 4; Fig. 5). The capacity for *P. nigra* to capture particulate matter (Table 4) reflects its considerably different adaxial and abaxial leaf surface micromorphologies (Fig. 5). For the ensiform leaves of *P. nigra*, PM density was statistically lower on their abaxial side for all fractions, being approximately a tenth of the median values from the adaxial side. In contrast, *H. helix* leaf sides did not show any significant difference in the median PM density, for any fraction. Finally, *T. occidentalis* was close to the significant difference threshold ($p < 0.05$) for TAP, most likely influenced by the higher and significantly different PM density of the adaxial leaf side for PM_1. The other fractions, $PM_{2.5}$ and PM_{10}, were more evenly distributed on both sides of *T. occidentalis* leaves (Fig. 5).

5 Discussion

The SEM imaging and 3D optical profilometry revealed considerable differences in the leaf micromorphology among species, as well as significant variations in their capacity to capture particles.

5.1 Leaf roughness and PM capture

Leaf surface roughness is frequently estimated as the quantification of grooves and ridges by estimating their width (2D distance measure), morphology or the proportion they cover of the leaf surface. This foliar characteristic is considered to have strong positive correlations with PM capture (Liang et al., 2016; Shao et al., 2019). In this study, an alternative measure of leaf roughness was used, namely areal average roughness denominated S_a, which is calculated from the leaves' 3D surface profiling and which takes into consideration the depth/height of the grooves/ridges (z axis) (Figs. 3,4). When looking purely at the effect of leaf surface micromorphology, roughness quantified without the influence of the leaf sample's broad curvature is preferred (S_a, Table 1), and it is discussed below.

Our study showed a weak relationship between PM capture and S_a on both, the adaxial and the abaxial, sides. *Thuja occidentalis* had the lowest surface roughness but showed the highest PM density, despite being located in the inner section of the green barrier. On the other hand, *P. nigra* had the highest leaf roughness; however, it showed the lowest PM density. *Hedera helix* was the only plant matching leaf roughness and PM density when compared to the other species. Shao et al., (2019), who used another 3D technique to calculate leaf roughness (confocal laser scanning microscopy), also found a weak relationship between abaxial surface roughness and the amount of PM on the leaves of 8 common garden plants from China. They calculated leaf roughness as the arithmetic average roughness of the leaf surface (R_a), i.e. the average difference between peaks and valleys; which is similar to S_a.

We explain the weak relationship between PM capture and S_a using the rationale that underpins the determination of S_a: surface height deviation from the mean line. The 3D micromorphology of certain leaf structures creates 'extremely high' deviation from the mean height line which, in turn, creates overall high S_a leaf roughness values. In other words, S_a quantifies the range of height/depth (z axis) change across a leaf, rather than focussing on local density or morphology of protuberances. For example, the abaxial surface of *P. nigra* showed a sizeable difference between S_v and S_p, that is to say, there is a large difference between its deepest groove and its tallest ridge, of 28.89 µm. This large S_v-S_p range causes high deviation from the mean surface height, and some of the extreme deep values correspond to the location of stomata, which are highly recurrent on the abaxial surface – *P. nigra* had the highest stomatal density. Examples of the extreme depth of *P. nigra* stomata and other deep structures of *H. helix* can be seen as deep blue areas in Figs. 3l and 3d, respectively.

The analysis shows that leaf roughness, computed as S_a, is not the optimum method to estimate PM capture by plant species. The 3D optical profiling analysis (Figs. 3,4), however, helped to understand the subtleties of PM adherence to the leaf surface. The total surface area does not directly correlate to PM capture; instead, the 3D analysis revealed that three leaf roughness descriptors: grooves' width, depth, and frequency, are relevant to PM capture (§4.1.3.2). The leaf surface area supports PM capture as long as its micromorphology (i.e., surface grooves) creates an accessible deposition area to the particles. Moreover, as Weerakkody et al. (2018) suggested, different groove types can perform better than others at PM capture as some would create more accessible deposition areas.

A key factor in PM capture is the relative size of the leaf surface grooves compared to the dimensions of the airborne particles. Consequently, here we define four groove types based on their combined groove width (x/y dimension in the leaf surface plane) and groove depth (z dimension perpendicular to leaf surface) dimensions. The groove widths here are described here as narrow (≤5 µm) or wide (>5 µm), whilst the z axis is described as shallow (≤2.5 µm) or deep (>2.5 µm). The four groove types have different PM capture potential, and their characteristics are as follows:

- Shallow/narrow: Grooves of ≤2.5 µm depth and ≤5 µm width. They have the potential to capture small PM, such as PM_1 and $PM_{2.5}$, dependant on the relative groove to particle size.
- Shallow/wide: Grooves of ≤2.5 µm depth and >5 µm width. Depending on the width dimension, this groove type might trap PM_{10} and it is not likely to be a good sink of PM_1 and $PM_{2.5}$ because the particles could be remobilised by surface airflow and subsequent incoming pollution particles.
- Deep/narrow: Grooves of >2.5 µm depth and ≤5 µm width. They can capture small PM and the depth of the groove can impede particles from being easily remobilised.
- Deep/wide: Grooves of >2.5 µm depth and >5 µm width. This type could trap larger PM sizes, from $PM_{2.5}$ to PM_{10}.

When PM particles are trapped in grooves which are wide enough for them to enter but narrow/deep enough to protect them from the main airflow/particle bombardment, then the probability of long-term adhesion increases. Because of the range of PM sizes, e.g., PM_1, $PM_{2.5}$, and PM_{10}, there are likely different optimum dimensions of leaf surface grooves to trap the different PM sizes and shapes, especially since larger particles, and particles with high aspect ratios such as fibres, cannot enter grooves that are smaller than themselves.

Based on its leaf roughness descriptors, *P. nigra* seems suited for capturing only small PM by its adaxial leaf side that predominantly has shallow/narrow grooves and some shallow/wide (Fig. 4e). This upper surface was able to accommodate more PM_1 than *H. helix*, and particles were found clustered around the irregularities of the leaf (Fig. 2i). Its abaxial surface has deep/wide and shallow/wide grooves, being up to 18 µm wide, which is much larger than the PM fractions studied. Consequently, the abaxial surface of *P. nigra* is not optimum for

PM adherence. *Hedera helix* had deep/narrow grooves on both leaf sides, of ≤5 to 10 µm width (Figs. 4a,b). Overall, its grooves were highly effective at trapping particles, especially the smaller PM_1 and $PM_{2.5}$, the grooves were very frequent, increasing its PM capture capacity. *Thuja occidentalis* had shallow/narrow grooves, except at and around stomata (Figs. 4c,d), but had the highest PM capture for all range of particle sizes. This indicates that other micromorphological traits, besides leaf roughness, also influence PM capture efficacy.

5.2 Other micromophological mechanisms affecting foliar PM capture

From the plants studied, *H. helix* seems to have the most conducive grooves for PM capture due to their size, shape, and frequency. Despite this, it was not the species with the greatest measured PM density. Instead, *T. occidentalis* had the highest PM density, where PM_1 and TAP density were statistically different between both species (Table 3). Therefore, the interaction of other macro and micromorphological traits and environmental factors can outweigh the influence of just one feature, in this case, foliar roughness, as suggested by Sgrigna et al. (2020).

The presence of wax on the leaves of *T. occidentalis* might partially explain its higher PM density compared to *H. helix*. Both species exhibited epicuticular waxes on both sides of the leaf; nevertheless, the wax layer on *T. occidentalis* was more prominent and visible in the SEM images (Fig 2g). The existence of a significant wax layer hindered leaf observation under high SEM magnifications due to local electron beam-induced melting, similar to the observations reported by Stabentheiner, Zankel and Pölt, (2010) on the conifer tree *Picea omorika*. Some studies have positively correlated wax on leaf surface, especially in conifer species, to their capacity to capture PM (Sæbø et al., 2012; Xu et al., 2019). Here, the notable wax layer on *T. occidentalis* appears to contribute to the adhesion and, therefore, immobilisation of the particles both in the grooves and additionally on top of ridges.

Some studies have reported hairy leaves as an effective mechanism to facilitate PM capture (Chiam et al., 2019; Wang et al., 2019). Here, only *P. nigra* had occasional microhairs (Figs. 2j,l), and the other species did not present any trichomes or hairs on their surface; therefore, it was not a significant PM capture mechanism in this study. Rather, the minimum presence and lack of this trait in the sampled foliage enabled a better understanding of the influence of the other micromorphological characteristics.

Divided opinions exist around the influence of stomata presence and density on PM capture, and no consent has been reached. For instance, Chen et al., (2017) did not find a correlation between stomatal density and $PM_{2.5}$ capture after assessing 15 tree species from Beijing; Liang et al. (2016) found low stomatal size species effective at $PM_{2.5}$ capture; whilst Sgrigna et al. (2020) considers stomatal density to be positively correlated to PM deposition and suggests that its presence might add to leaf roughness. As depicted in Fig. 2b, a large number of particles (PM_1 and $PM_{2.5}$) were found locally adhered in the deep/narrow grooves around the edges of *H. helix* stomata; which was not the case for *P. nigra,* nor for *T. occidentalis*. The latter had the highest PM density but lowest stomatal density. On the contrary, *P. nigra* had the lowest PM density and highest stomatal density. The evidence here, from detailed 3D microstructural analyses, indicates that stomatal density will only have a positive correlation with PM capture if the grooves that surround the stoma have the right depth and width for the particles to be trapped, such being the case of *H. helix* (Fig 2b).

5.3 Species variation in PM capture

The studied species performed differently at PM capture within the same green barrier. They can be ranked based on their overall PM density performance from highest to lowest as follows: *Thuja occidentalis* > *Hedera helix* > *Phyllostachys nigra* (Fig. 5). For all the samples analysed, the overall particle count of PM_1 was at least 5 times higher than $PM_{2.5}$, and $PM_{2.5}$ was four times higher than PM_{10}. The significantly higher PM_1 density adhered to *T. occidentalis* meant it was the top-ranked leaf-type in overall PM density performance from all species (Table 3).

All species had in common that the larger the pollution particle size, the lower the proportion of particles adhered on the leaves, which matches previous findings from Ottelé et al. (2010) and Weerakkody et al. (2017). Our observation of a lower frequency of adhered $PM_{2.5}$ and PM_{10} particles compared to PM_1 particles correlates both with the reduced number of suitably sized grooves which can effectively trap the larger PM_{10} particles, and the reduced efficacy of surface adherence by wax for heavier particulates. Other studies (Przybysz et al., 2014; Song et al., 2015) differ from the particle distribution found here, finding PM_{10} to be the most abundant fraction, due in part because their equivalent PM proportion calculation method is based on the gravimetric rinsing, filtering and weighing approach by Dzierżanowski et al., (2011). Tomson et al. (2021) found significant drawbacks from the gravimetric particle analysis approach and recommend using microscopy imaging techniques over gravimetric.

It is worth noting that PM density and distribution on the leaf samples are not equal to the atmospheric PM concentrations of the study area. PM pollution present on the leaves depends on impact (incoming flux, weather, green barrier design), adherence (e.g. leaf performance) and removal (incoming flux/impacts, weather). Additionally, there is a biological interaction between the PM compounds and the leaves, which might lead to the absorption/transformation of pollutants; for instance, of compounds containing nitrogen. Therefore, the adhered PM on the leaves is not identical to airborne pollution concentrations.

In this study, *T. occidentalis* and *P. nigra* were located immediately behind a *H. helix* fence, comprising together a section of the green barrier. There is a possibility of direct wind shadowing by the *Hedera* climber on the *T. occidentalis* and *P. nigra* specimens, or other disruptions to air flow patterns caused by the *Hedera* leaves and the gaps between these leaves (hedges and facades are thought to slow wind speed, not block air movement entirely, Chang, 2006). However, despite their location, all plants showed foliar PM deposition. In fact, *T. occidentalis* had the highest PM density for all fractions, meaning that its micromorphological mechanisms for PM capture outweigh the spatial conditions. Other studies have also found that conifers perform strongly at PM capture. For instance, another scale-like conifer, *Thuja plicata* was highly rated by Muhammad, Wuyts and Samson (2019), based on its leaf saturation isothermal remanent magnetisation (SIRM), a proxy for induced particle accumulation. Additionally, species from the *Pinus* and *Juniperus* genus have also shown superior particle adherence compared to broadleaved species (Przybysz et al., 2014; Zhang et al., 2018).

Here, *P. nigra* had the lowest PM density of the three analysed species but still was effective in collecting airborne particles, especially PM_1, despite being in the inner side of the green barrier. Some studies have shown that other bamboo plants capture $PM_{2.5}$ and PM_{10}, such as *Phyllosthachys bissetti* (Morina et al., 2013), or can lower the atmospheric concentrations of these contaminants, such as a *Phyllostachys edulis* forest in China (Bi et al., 2018). The *P. nigra* specimens in our study also helped shape the green barrier and make it denser, which is highly important for the deflection effect of the barrier on air pollution (Tomson et al., 2021).

Analysis of both the adaxial and abaxial sides of each leaf type clarifies the contribution of each surface to the overall particle capture efficacy. The most notable effect was found for *P. nigra*, where the PM load on its abaxial surface was significantly lower than the opposite side for all PM fractions, being approximately a tenth of the median values from the adaxial side (Table 4). This marked difference clearly affected its PM capture performance, which otherwise could have been similar to *H. helix* performance since the adaxial side of both species exhibited similar PM densities. Our results for *H. helix* are aligned to the findings of Weerakkody et al. (2017), where the adaxial surface had significantly higher values; which is true for $PM_{2.5}$, PM_{10} and TAP from our sample.

Overall, we found that all examined green barrier species captured PM through the action of multiple mechanisms afforded by the range of leaf micromorphologies at the first and second layer of the green barrier. *Hedera helix* is an effective first layer for PM capture, which seems to be suited for PM_1 and $PM_{2.5}$ adherence due to optimum groove size and frequency. In the second layer, *T. occidentalis* possess a wax layer that enables it to capture a significantly higher number of particles, and *P. nigra* serves as a structural plant for PM deflection, and its adaxial side seems to adequately capture PM_1. Abhijith and Kumar (2020) suggest that multiple row green barriers should have the most pollution-tolerant species located closer to the pollution source, as per *H. helix* in our study. In addition to their findings, our results suggest that having a mixed green barrier fosters multiple opportunities to capture PM, potentially more when compared to a single species green barrier.

5.4 3D optical profilometry in air quality science

The combination of the leaf examination techniques used in this study, specifically SEM paired with 3D optical profilometry, has contributed to a new understanding of the various mechanisms by which PM is deposited and retained on the foliage of three species once the macromorphological and environmental barriers have been overcome. Even though the determination of S_a leaf surface roughness was not found to be an optimum method to predict PM density, 3D optical profilometry is shown to be advantageous since it enables the detailed determination of localised leaf roughness/3D surface morphology on a size-scale similar to the PM particle size. The combined techniques have determined that 1) leaf micromorphology is highly heterogeneous on the nm-10μm size scale; 2) leaf roughness descriptors: grooves' width, depth and frequency, strongly influence PM capture and retention; and 3) stomatal density is not correlated to PM capture unless the surface surrounding the stomata has the ideal size and shape for PM capture. Further research on leaf roughness descriptors should be undertaken for more species to complement our observations.

6 Conclusion

The capture of airborne pollution particles by leaves is influenced by plant micromorphological traits, which determine the mechanisms for PM capture. In our study, the most conducive PM capture mechanisms were leaf roughness and the presence of wax.

Macro and microscale 3D leaf roughness was determined using 3D optical profilometry, which is a new method for the analysis of air pollution mitigation by plants. It was found that the roughness parameter S_a was not an optimum method to predict PM capture due to certain localised structures, such as stomata, causing high deviation from the mean leaf height, and producing high S_a that did not reflect the leaf surface conditions. Nevertheless, the 3D optical profilometry spatial maps and linescans, helped to identify the leaf roughness descriptors that most influenced PM deposition: namely grooves' width, depth, and frequency. The total surface area of the leaves did not directly correlate to PM deposition, instead, particle capture is influenced by the accessible area to the particles due to the leaf surface structures (i.e., surface grooves). For the range of analysed PM sizes, i.e. PM_1, $PM_{2.5}$, and PM_{10}, there are likely different optimum dimensions of leaf surface grooves to trap the different PM sizes and shapes. The descriptors clarified the suitability of *H. helix* for capturing PM_1 and $PM_{2.5}$ through frequent deep/narrow grooves, predominantly smaller than PM_{10} particles. In contrast, atmospheric PM primarily adhered to *T. occidentalis* leaves due to its abundant wax layer. Stomatal density did not seem to foster enhanced PM deposition unless the grooves surrounding the stoma/guard cells were of the right depth and width to accommodate the particles.

The green barrier species, *Hedera helix* 'Woerner', *Thuja occidentalis* 'Smaragd', and *Phyllostachys nigra*, were examined under the SEM and all showed to have captured PM pollution. The SEM method used here is effective to a resolution limit of 0.2 μm, and further work could explore the <0.2 μm particle capture by plants to investigate air quality gains at a lower scale.

For all three species, PM_1 was the most numerically abundant fraction adhered to the leaves, accounting for approximately 80% of all particles and followed in descending order by $PM_{2.5}$ and PM_{10}. *Thuja occidentalis* had the highest PM areal number density, having captured double the TAP of *H. helix* and triple of *P. nigra*, despite being located behind the ivy (*Hedera*) climber. *Phyllostachys nigra* had the lowest relative PM load, but it still has significant potential for air quality remediation, both for PM_1 capture and for pollution deflection as a plant that adds structure to the green barrier. The use of multiple plant species in the green barrier allows the concurrent action of multiple PM capture mechanisms and enables PM capture by leaf topology to occur at different size scales, fostering more opportunities to capture PM than using only one species for air filtering.

The study of foliar surface roughness and other micromorphological features helps to account for the subtle differences among plants in terms of their air cleaning capacity and to guide the selection of the best plant combinations to reduce air pollution and improve citizens' health. The use of 3D optical profiling is shown to enable a better understanding of the influence of leaf roughness/morphology on PM capture and retention, with 3D leaf surface height maps providing detailed information on the leaf surface structure at the scale of the pollution particles, thereby locating the places and structures most conducive for PM deposition.

7 Declaration of interest

The authors declare that they have no known competing financial interests or personal relationships that could have appeared to influence the work reported in this paper.

8 Acknowledgements

The authors acknowledge the support of the Grantham Centre for Sustainable Futures, The University of Sheffield for a PhD studentship (MCRB); The Turkish Government for a PhD studentship (ITG); The Urban Flows Observatory, The University of Sheffield for the deployment of the air quality monitor, weather station, and access to traffic data; and Hunter's Bar Infant School, Sheffield, for green barrier permissions. The Henry Royce Institute for Advanced Materials, funded through EPSRC grants EP/R00661X/1, EP/S019367/1, EP/P02470X/1 and EP/P025285/1, is acknowledged for Contour Elite access at Royce@Sheffield.

9 Author Contributions

MCRB: conceptualisation, methodology, SEM investigation, SEM and optical profilometry analysis, writing - original draft and editing. ITG: optical profilometry investigation and analysis. RWC: supervision, green barrier conceptualisation, writing - reviewing and editing. BJI: conceptualisation, resources, analysis, and writing - reviewing and editing.

10 References

Abhijith, K. V., Kumar, P., 2020. Quantifying particulate matter reduction and their deposition on the leaves of green infrastructure. Environ. Pollut. 265, 114884. https://doi.org/10.1016/j.envpol.2020.114884

Beentje, H., 2020. The Kew Plant Glossary: an illustrated dictionary of plant terms, Second. ed. Royal Botanic Gardens, Kew, Richmond.

Bi, Y.F., Guo, F.Y., Yang, L., Zhong, H., Wang, A.K., Wang, Y.K., Wu, Z.Z., Du, X.H., 2018. Phyllostachys edulis forest reduces atmospheric PM2.5 and PAHs on hazy days at suburban area. Sci. Rep. 8, 1–11. https://doi.org/10.1038/s41598-018-30298-9

Chang, W.R., 2006. Effect of porous hedge on cross ventilation of a residential building. Build. Environ. 41, 549–556. https://doi.org/10.1016/j.buildenv.2005.02.032

Chen, J., Yu, X., Bi, H., Fu, Y., 2017. Indoor simulations reveal differences among plant species in capturing particulate matter. PLoS One 12, 1–22. https://doi.org/https://doi.org/10.1371/journal.pone.0177539

Chen, L., Liu, C., Zhang, L., Zou, R., Zhang, Z., 2017. Variation in Tree Species Ability to Capture and Retain Airborne Fine Particulate Matter (PM2.5). Sci. Rep. 7, 1–11. https://doi.org/10.1038/s41598-017-03360-1

Chiam, Z., Song, X.P., Lai, H.R., Tan, H.T.W., 2019. Particulate matter mitigation via plants: Understanding complex relationships with leaf traits. Sci. Total Environ. 688, 398–408. https://doi.org/10.1016/j.scitotenv.2019.06.263

Drake, P.L., de Boer, H.J., Schymanski, S.J., Veneklaas, E.J., 2019. Two sides to every leaf: water and CO2 transport in hypostomatous and amphistomatous leaves. New Phytol. 222, 1179–1187. https://doi.org/10.1111/nph.15652

Dzierżanowski, K., Popek, R., Gawrońska, H., Sæbø, A., Gawroński, S.W., 2011. Deposition of particulate matter of different size fractions on leaf surface and in waxes of urban forest species. Int. J. Phytoremediation 13, 1037–1046. https://doi.org/http://doi.org/10.1080/15226514.2011.552929

European Commission, 2015. Towards an EU Research and Innovation policy agenda for Nature-Based Solutions & Re-Naturing Cities. Brussels.

Harrison, R.M., 2020. Airborne particulate matter. Philos. Trans. R. Soc. A 378. https://doi.org/http://dx.doi.org/10.1098/rsta.2019.0319

He, C., Qiu, K., Alahmad, A., Pott, R., 2020. Urban Forestry & Urban Greening Particulate matter capturing capacity of roadside evergreen vegetation during the winter season. Urban For. Urban Green. 48, 126510. https://doi.org/10.1016/j.ufug.2019.126510

Hewitt, C.N., Ashworth, K., Mackenzie, A.R., 2019. Using green infrastructure to improve urban air quality (GI4AQ). Ambio. https://doi.org/10.1007/s13280-019-01164-3

Hutchings, I., Shipway, P., 2017. Surface topography and surfaces in contact, in: Tribology: Friction and Wear of Engineering Materials. Butterworth-Heinemann, Elsevier Ltd., Oxford, p. 17. https://doi.org/10.1016/B978-0-08-100910-9.00002-7

Liang, D., Ma, C., Wang, Yun-qi, Wang, Yu-jie, Chen-xi, Z., 2016. Quantifying PM2.5 capture capability of greening trees based on leaf factors analyzing. Environ. Sci. Pollut. Res. 23, 21176–21186. https://doi.org/10.1007/s11356-016-7687-9

McDonald, A.G., Bealey, W.J., Fowler, D., Dragosits, U., Skiba, U., Smith, R.I., Donovan, R.G., Brett, H.E., Hewitt, C.N., Nemitz, E., 2007. Quantifying the effect of urban tree planting on concentrations and depositions of PM10 in two UK conurbations. Atmos. Environ. 41, 8455–8467. https://doi.org/10.1016/j.atmosenv.2007.07.025

McDonald, R., Kroeger, T., Boucher, T., Longzhu, W., Salem, R., 2016. Planting Healthy Air.

Morina, F., Jovanović, L., Vidović, M., Sužnjević, D., Tripković, D., Milić, S., Srećković, T., Jovanović, S.V., 2013. Antioxidative status and acclimatization capacity of bamboo - Potential use for air quality improvement in urban areas. Fresenius Environ. Bull. 22, 1763–1769.

Muhammad, S., Wuyts, K., Nuyts, G., De Wael, K., Samson, R., 2020. Characterization of epicuticular wax structures on leaves of urban plant species and its association with leaf wettability. Urban For. Urban Green. 47, 126557. https://doi.org/10.1016/j.ufug.2019.126557

Muhammad, S., Wuyts, K., Samson, R., 2019. Atmospheric net particle accumulation on 96 plant species with contrasting morphological and anatomical leaf characteristics in a common garden experiment. Atmos. Environ. 202, 328–344. https://doi.org/10.1016/j.atmosenv.2019.01.015

Ottelé, M., Bohemen, H.D. Van, Fraaij, A.L.A., 2010. Quantifying the deposition of particulate matter on climber vegetation on living walls. Ecol. Eng. 36, 154–162. https://doi.org/10.1016/j.ecoleng.2009.02.007

Przybysz, A., Sæbø, A., Hanslin, H.M., Gawroński, S.W., 2014. Accumulation of particulate matter and trace elements on vegetation as affected by pollution level, rainfall and the passage of time. Sci. Total Environ. 481, 360–369. https://doi.org/10.1016/j.scitotenv.2014.02.072

R Core Team, 2020. R: A language and environment for statistical computing, R Foundation for Statistical Computing. Vienna, Austria.

Sæbø, A., Popek, R., Nawrot, B., Hanslin, H.M., Gawronska, H., Gawronski, S.W., 2012. Plant species differences in particulate matter accumulation on leaf surfaces. Sci. Total Environ. 427–428, 347–354. https://doi.org/10.1016/j.scitotenv.2012.03.084

Schindelin, J., Arganda-Carreras, I., Frise, E., Kaynig, V., Longair, M., Pietzsch, T., Preibisch, S., Rueden, C., Saalfeld, S., Schmid, B., Tinevez, J.-Y., White, D.J., Hartenstein, V., Eliceiri, K., Tomancak, P., Cardona, A., 2012. Fiji: an open-source platform for biological-image analysis. Nat. Methods 9, 676–682. https://doi.org/10.1038/nmeth.2019

Sgrigna, G., Baldacchini, C., Dreveck, S., Cheng, Z., Calfapietra, C., 2020. Relationships between air particulate matter capture efficiency and leaf traits in twelve tree species from an Italian urban-industrial environment. Sci. Total Environ. 718, 137310. https://doi.org/10.1016/j.scitotenv.2020.137310

Shao, F., Wang, L., Sun, F., Li, G., Yu, L., Wang, Y., Zeng, X., Yan, H., Dong, L., Bao, Z., 2019. Study on different particulate matter retention capacities of the leaf surfaces of eight common garden plants in Hangzhou, China. Sci. Total Environ. 652, 939–951. https://doi.org/10.1016/j.scitotenv.2018.10.182

Song, Y., Maher, B.A., Li, F., Wang, X., Sun, X., Zhang, H., 2015. Particulate matter deposited on leaf of five evergreen species in Beijing, China: Source identification and size distribution. Atmos. Environ. 105, 53–60. https://doi.org/10.1016/j.atmosenv.2015.01.032

Stabentheiner, E., Zankel, A., Pölt, P., 2010. Environmental scanning electron microscopy (ESEM)-a versatile tool in studying plants. Protoplasma 246, 89–99. https://doi.org/10.1007/s00709-010-0155-3

Tomson, M., Kumar, P., Barwise, Y., Perez, P., Forehead, H., French, K., Morawska, L., Watts, J.F., 2021. Green infrastructure for air quality improvement in street canyons. Environ. Int. 146, 106288. https://doi.org/10.1016/j.envint.2020.106288

Urban Flows Observatory at The University of Sheffield, 2020. Traffic data from the Urban Flows Observatory. https://doi.org/https://doi.org/10.15131/shef.data.13066661.v2

Vieira, R.C., Gomes, D.M.S., Sarahyba, L.S., Arruda, R.C.O., 2002. Leaf anatomy of three herbaceous bamboo species. Brazilian J. Biol. 62, 907–922.

Wang, H., Maher, B.A., Ahmed, I.A.M., Davison, B., 2019. Efficient removal of ultrafine particles from diesel exhaust by selected tree species: implications for roadside planting for improving the quality of urban air. Environ. Sci. Technol. 53, 6906–6916. https://doi.org/10.1021/acs.est.8b06629

Weerakkody, U., Dover, J.W., Mitchell, P., Reiling, K., 2018a. Evaluating the impact of individual leaf traits on atmospheric particulate matter accumulation using natural and synthetic leaves. Urban For. Urban Green. 30, 98–107. https://doi.org/10.1016/j.ufug.2018.01.001

Weerakkody, U., Dover, J.W., Mitchell, P., Reiling, K., 2018b. Quantification of the traffic-generated particulate matter capture by plant species in a living wall and evaluation of the important leaf characteristics. Sci. Total Environ. 635, 1012–1024. https://doi.org/https://doi.org/10.1016/j.sdtotenv.2018.04.106

Weerakkody, U., Dover, J.W., Mitchell, P., Reiling, K., 2017. Particulate matter pollution capture by leaves of seventeen living wall species with special reference to rail-traffic at a metropolitan station. Urban For. Urban Green. 27, 173–186. https://doi.org/10.1016/j.ufug.2017.07.005

WHO, 2019. Ambient air pollution: Pollutants [WWW Document]. URL https://www.who.int/airpollution/ambient/pollutants/en/ (accessed 8.2.19).

Xiong, D., Flexas, J., 2020. From one side to two sides: the effects of stomatal distribution on photosynthesis. New Phytol. 1–13. https://doi.org/10.1111/nph.16801

Xu, H., Wang, W., Wang, H., Sun, Y., Zhong, Z., Wang, S., 2019. Differences in quantity and composition of leaf particulate matter and morphological structures in three evergreen trees and their association in Harbin, China. Environ. Pollut. 252, 1772–1790. https://doi.org/10.1016/j.envpol.2019.06.124

Yigit, N., 2017. Micromorphological studies on plants and their importance, in: Developments in Science and Engineering. Sofia.

Zhang, L., Zhang, Z., Chen, L., McNulty, S., 2019. An investigation on the leaf accumulation-removal efficiency of atmospheric particulate matter for five urban plant species under different rainfall regimes. Atmos. Environ. 208, 123–132. https://doi.org/10.1016/j.atmosenv.2019.04.010

Zhang, W., Zhang, Z., Meng, H., Zhang, T., 2018. How does leaf surface micromorphology of different trees impact their ability to capture particulate matter? Forests 9. https://doi.org/10.3390/f9110681

11 Tables and figures

Figure 1. Images of the green barrier section used for the study in February 2020. Plants viewed from the school playground (a) front and (b) side view: (c) plants viewed from the street.

Table 1. Leaf roughness and stomatal density of plant species measured by 3D optical profilometry, (1) With curvature from leaf as mounted in ContourGT, and (2) Broad leaf curvature removed by Gaussian filter.

Species	Stomatal density	Leaf side	1) With curvature (µm)			2) Leaf curvature removed (µm)		
			S_a	S_p	S_v	S_a	S_p	S_v
H. helix	207.69 ± 9.30 stoma mm^{-2}	adaxial	2.37	7.47	-21.54	0.77	5.34	-18.20
		abaxial	2.57	8.16	-23.39	1.23	5.72	-20.53
T. occidentalis	36.82 ± 12.43 stoma mm^{-2}	adaxial	4.10	12.71	-15.29	0.63	5.54	-11.60
		abaxial	3.06	11.30	-9.20	0.49	2.52	-2.27
P. nigra	413.49 ± 21.19 stoma mm^{-2}	adaxial	1.39	8.41	-9.72	0.83	4.36	-13.82
		abaxial	2.84	14.09	-18.68	2.57	11.12	-17.77

S_a = areal average roughness, S_p = maximum peak height, S_v = maximum valley depth, stomatal density values are calculated as mean ± SE of both adaxial and abaxial sides.

Table 2. Particle count and proportion of PM_1, $PM_{2.5}$ and PM_{10} observed on the leaves, per species.

Species	Leaf side	Particle count			Proportion		
		PM_1	$PM_{2.5}$	PM_{10}	PM_1	$PM_{2.5}$	PM_{10}
H. helix	adaxial	1,142	366	54	83.61%	14.29%	2.11%
	abaxial	1,210	333	146	71.43%	19.66%	8.62%
	both	3,352	699	200	78.76%	16.42%	4.70%
T. occidentalis	adaxial	3,482	433	138	85.74%	10.66%	3.40%
	abaxial	1,341	197	43	84.77%	12.45%	2.72%
	both	4,823	630	181	85.47%	11.16%	3.21%
P. nigra	adaxial	1,133	255	32	79.79%	17.96%	2.25%
	abaxial	140	23	3	84.34%	13.86%	1.81%
	both	1,273	278	35	80.26%	17.53%	2.21%

The remaining proportion to complete 100% corresponds to particles of more than 10 µm in size, which is less than 0.14% in average for *H. helix* and *T. occidentalis* species. *Phyllostachys nigra* did not show adherence of any particles above 10 µm diameter.

Table 3. Median (IQR) PM density (1x10^2 mm^2) of PM_1, $PM_{2.5}$ and PM_{10} observed per species, combined for abaxial and adaxial surfaces, and inter-species variation.

Species	PM_1		$PM_{2.5}$		PM_{10}		TAP	
	Median (IQR)	H(2) = 18.84 $p < 0.05$	Median (IQR)	H(2) = 12.84 $p < 0.05$	Median (IQR)	H(2) = 9.43 $p < 0.05$	Median (IQR)	H(2) = 17.32 $p < 0.05$
H. helix	**24.30** (18.99-56.63)	a	**12.32** (6.67-25.53)	ab	**2.12** (0.89-7.05)	ab	**42.74** (26.76-88.15)	a
T. occidentalis	**76.47** (57.95-101.45)	b	**19.03** (13.93-26.51)	a	**3.06** (2.21-4.25)	a	**93.46** (84.11-132.20)	b
P. nigra	**24.30** (3.06-39.25)	a	**3.40** (1.87-11.72)	b	**0.51** (0.34-2.21)	b	**28.21** (4.59-49.28)	a

Species that share the same letter have PM density values that are not significantly different from each other, according to post hoc Dunn's test. TAP=Total Adhered Particles, total sum of the PM categories.

Table 4. Median (IQR) PM density (1x10^2 mm^2) of PM_1, $PM_{2.5}$ and PM_{10} for plants' adaxial and abaxial leaf surfaces.

PM fraction	Leaf side	*H. helix*	*T. occidentalis*	*P. nigra*
PM_1	adaxial	**22.43** (20.90-78.17)	**104.25** (75.96-143.93)	**39.25** (29.23-68.14)
	abaxial	**27.86** (18.35-40.95)	**71.19** (48.77-78.17)	**2.71** (2.21-4.29)
			* W=14, $p < 0.035$	* W=0, $p < 0.0006$
$PM_{2.5}$	adaxial	**17.84** (9.01-27.87)	**26.42** (13.89-43.71)	**11.72** (8.67-14.44)
	abaxial	**8.84** (6.63-18.01)	**16.31** (13.93-20.73)	**1.36** (0.42-2.25)
				* W=0.5, $p < 0.0007$
PM_{10}	adaxial	**2.38** (1.36-5.78)	**3.23** (2.17-12.45)	**2.21** (1.19-4.08)
	abaxial	**1.87** (0.68-7.48)	**2.89** (2.38-4.25)	**0.25** (0.0-0.38)
				* W=4, $p < 0.002$
TAP	adaxial	**50.30** (29.06-98.73)	**146.31** (92.02-192.02)	**49.28** (37.55-82.75)
	abaxial	**35.17** (26.00-81.40)	**90.23** (60.66-105.86)	**4.33** (3.57-5.86)
			W=16, $p < 0.059$	* W=0, $p < 0.0006$

* represents significant differences of PM density between both sides of the leaves, according to Wilcoxon rank sum test. TAP=Total Adhered Particles, total sum of the PM categories.

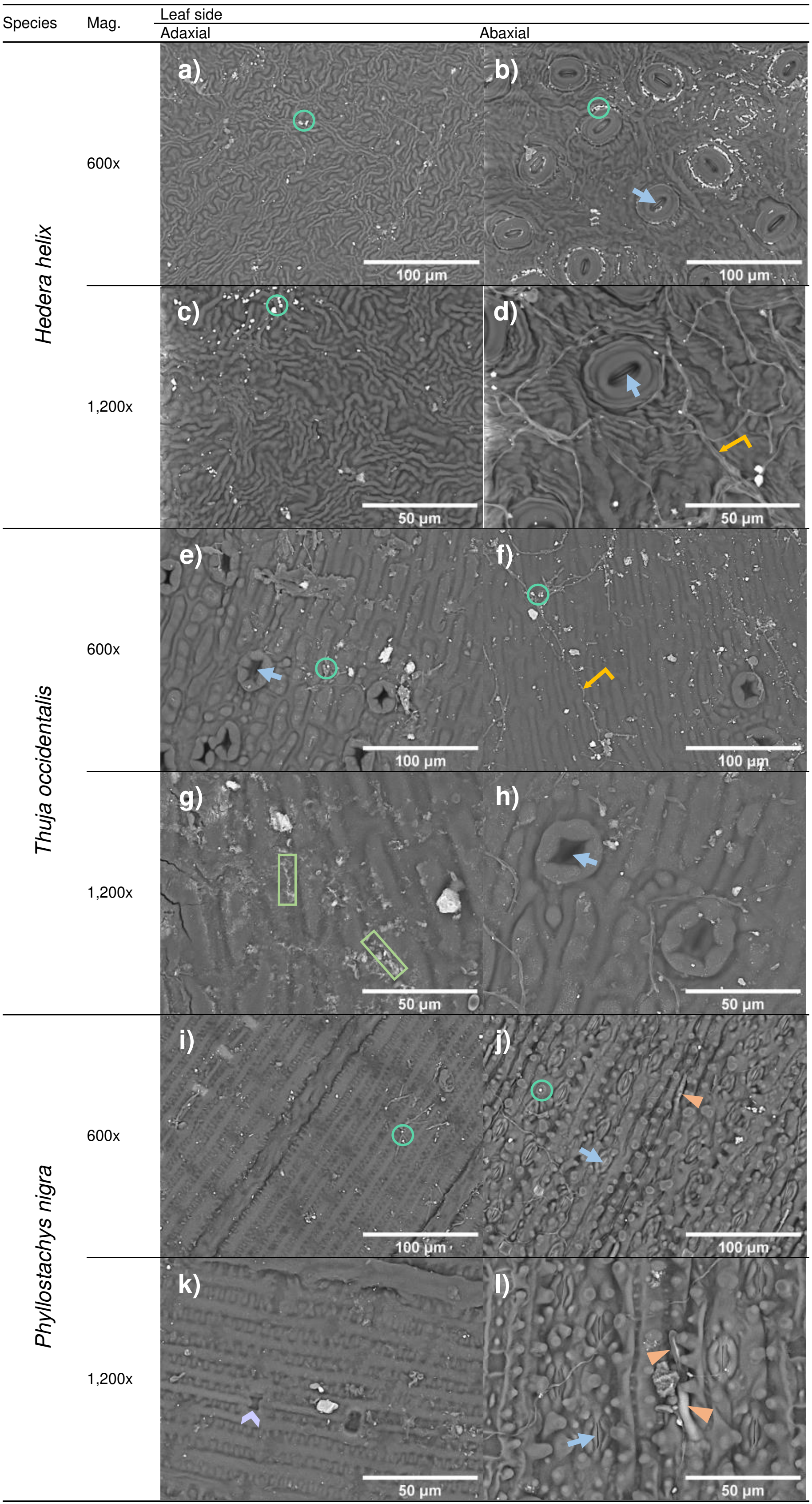

Figure 2. SEM BSE images of leaf samples exposed to PM pollution, shown by species and magnification (Mag.). (a-d) *Hedera helix*, (e-h) *Thuja occidentalis*, (i-l) *Phyllostachys nigra*. Linear blue arrows point at examples of stomata; L-shaped arrows point at fibres network; triangles point at leaf microhairs and a chevron points at a potential silica body of *P. nigra*; circles encapsulate examples of adhered particulate matter and rectangles encapsulate examples of melted wax in *T. occidentalis*.

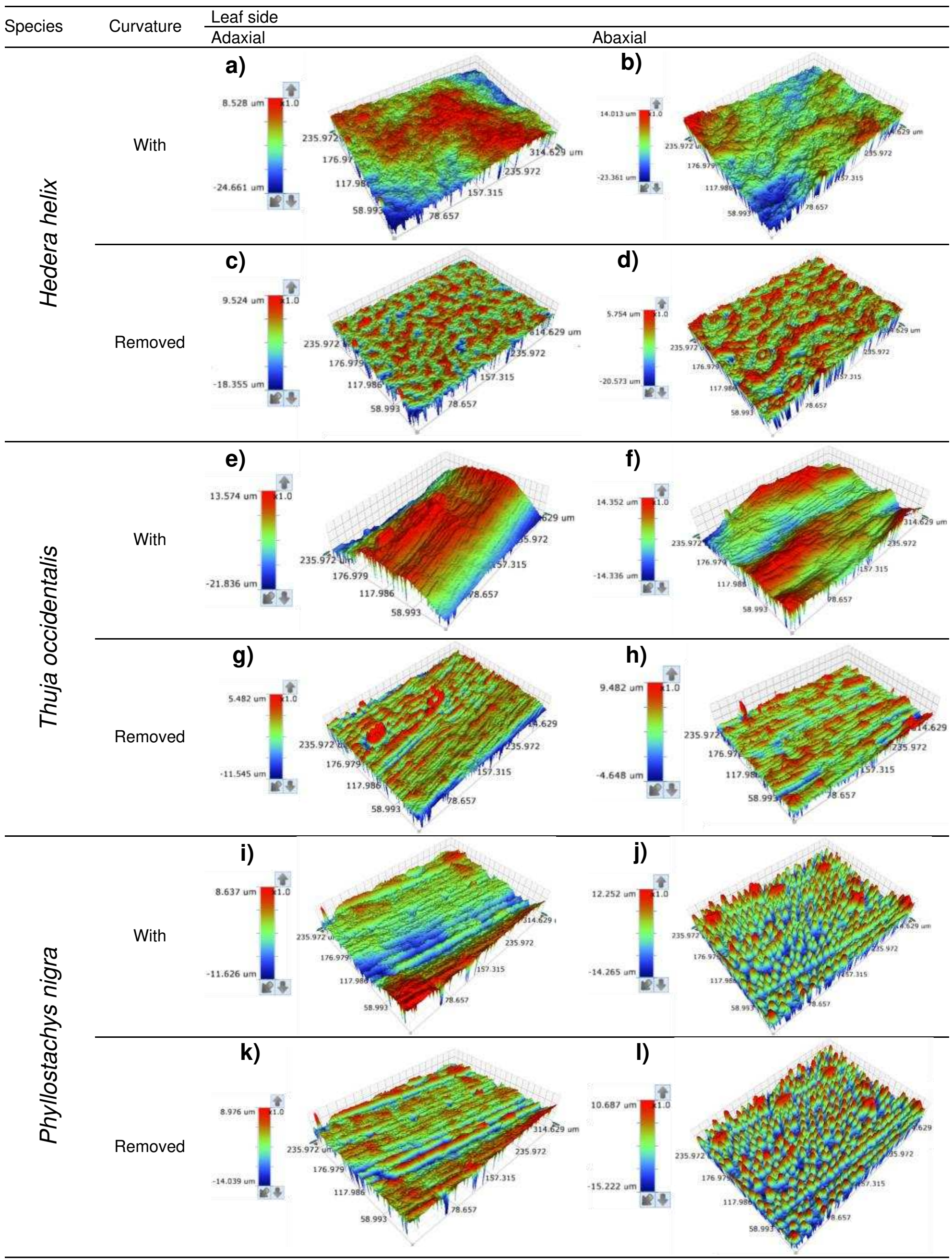

Figure 3. Leaf surface topography: 3D profiles of adaxial and abaxial leaf surfaces measured by optical profilometry, shown with the curvature of the leaf as mounted ('With'), and with underlying curvature removed by Gaussian filter to show solely the local micromorphology of the leaf surface ('Removed'). (a-d) *Hedera helix*, (e-h) *Thuja occidentalis*, (i-l) *Phyllostachys nigra*. **Note: colour figure.**

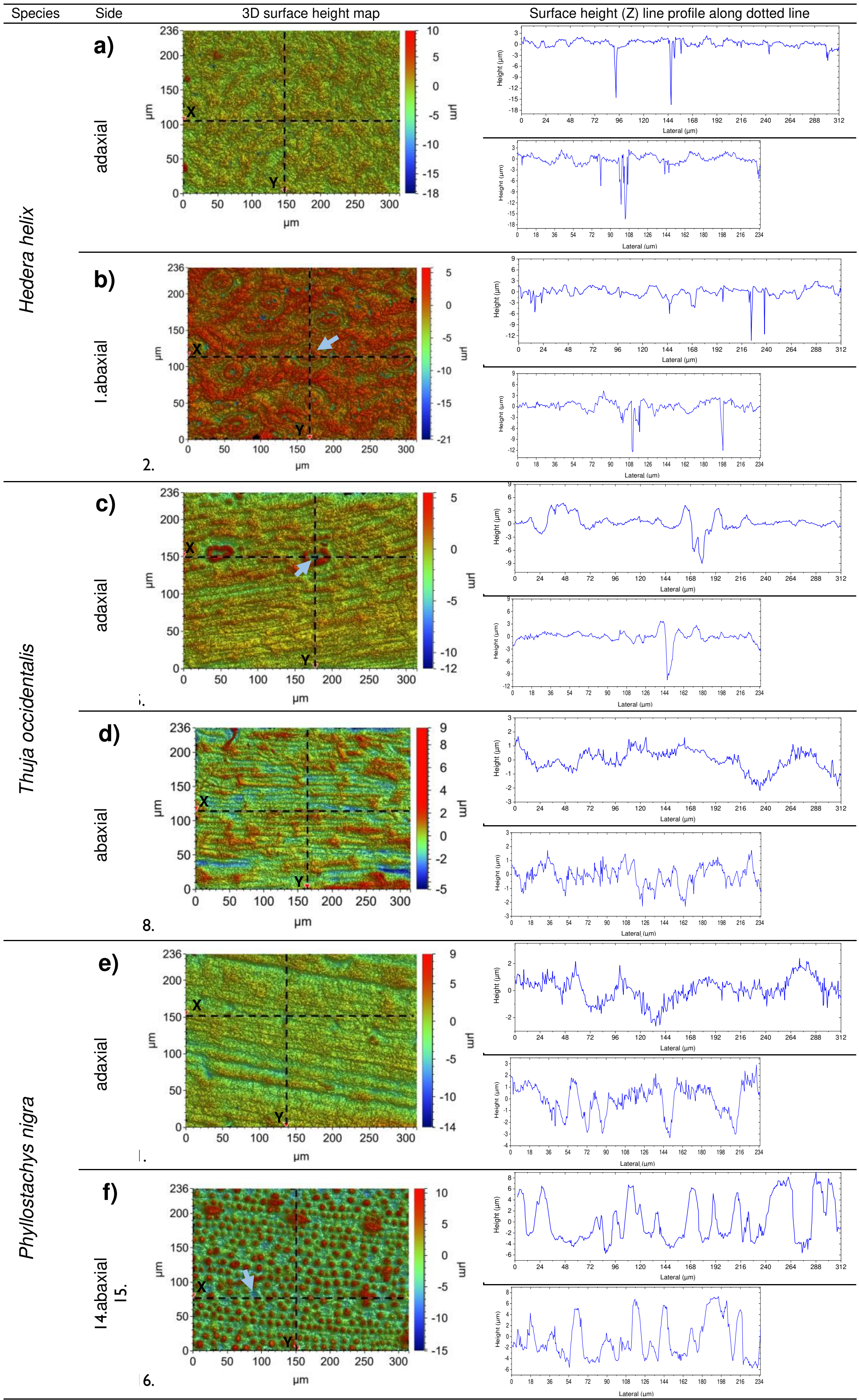

Figure 4. Leaf surface topography shown by 3D optical profilometry surface height maps (left; curvature removed) of adaxial and abaxial leaf surfaces (a-b) *Hedera helix*, (c-d) *Thuja occidentalis*, (e-f) *Phyllostachys nigra*. Linear blue arrows point at examples of stomata. Surface height line profiles (right), illustrate the variation in surface height due to micromorphological leaf traits such as grooves and stomata along two perpendicular directions (X, Y dotted lines). **Note: colour figure.**

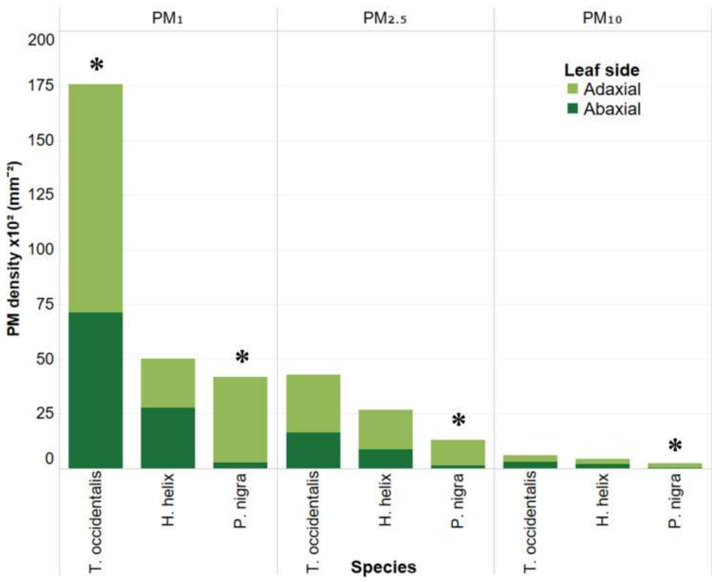

Figure 5. Median PM density of PM_1, $PM_{2.5}$ and PM_{10} identified on the adaxial and abaxial surfaces of each green barrier plant species, in descending order. IQR not shown for clarity. * Indicates statistical differences between the adaxial and abaxial surfaces of the same species.